

Binary black hole merger in the extreme mass ratio limit

Alessandro Nagar¹, Thibault Damour², and Angelo Tartaglia¹

¹ Dipartimento di Fisica, Politecnico di Torino, Corso Duca degli Abruzzi 24, 10129 Torino, Italy and INFN, sez. di Torino, Via P. Giuria 1, Torino, Italy

² Institut des Hautes Etudes Scientifiques, 35 route de Chartres, 91440 Bures-sur-Yvette, France

Abstract. We discuss the transition from quasi-circular inspiral to plunge of a system of two nonrotating black holes of masses m_1 and m_2 in the extreme mass ratio limit $m_1 m_2 \ll (m_1 + m_2)^2$. In the spirit of the Effective One Body (EOB) approach to the general relativistic dynamics of binary systems, the dynamics of the two black hole system is represented in terms of an effective particle of mass $\mu \equiv m_1 m_2 / (m_1 + m_2)$ moving in a (quasi-)Schwarzschild background of mass $M \equiv m_1 + m_2$ and submitted to an $\mathcal{O}(\mu)$ radiation reaction force defined by Padé resumming high-order Post-Newtonian results. We then complete this approach by numerically computing, à la Regge-Wheeler-Zerilli, the gravitational radiation emitted by such a particle. Several tests of the numerical procedure are presented. We focus on gravitational waveforms and the related energy and angular momentum losses. We view this work as a contribution to the matching between analytical and numerical methods within an EOB-type framework.

PACS numbers: 04.25.Dm, 04.30.Db, 04.70.Bw, 95.30.Sf, 97.60.Lf

Submitted to: *Class. Quantum Grav.*

1. Introduction

The last months have witnessed a decisive advance in Numerical Relativity, with different groups being able to simulate, for the first time and by using different techniques, the merger of two black holes of comparable masses (without or with initial spin) [1, 2, 3, 4]. Since such binary black holes systems (of a total mass $\sim 30M_\odot$) are believed to be among the most promising sources of gravitational waves for the ground based detectors like LIGO and VIRGO, this breakthrough raises the hope to have, for the first time, a reliable estimate of the complete waveform by joining together Post-Newtonian (PN) and Numerical Relativity results. We recall that PN techniques have provided us with high-order results for describing the motion [6, 7] and radiation [8, 9] of binary systems, and that further techniques have been proposed for *resumming* the PN results [10, 11, 12], thereby allowing an analytical description of the gravitational waveform emitted during the transition between inspiral and plunge, and even during the subsequent merger and ringdown phases. We now face the important task of constructing accurate *complete waveforms* by *matching* together the information contained in *Post-Newtonian* and *Numerical Relativity* results. We view the present work as a contribution towards this goal (for a recent first cut at this problem see [13, 14, 15]).

The work we present here belongs to a scientific lineage which started with the pioneering works of Regge and Wheeler [16], Zerilli [17], Davis, Ruffini, Press and Price [18]

and Davis, Ruffini and Tiomno [19]. References [18, 19] studied the gravitational wave emission due to the *radial plunge* (from infinity) of a particle onto a Schwarzschild black hole. This was thought of as a model for the head-on collision of two black holes in the extreme mass ratio limit. The gravitational wave energy spectrum [18] and waveform [19] were obtained. Davis, Ruffini and Tiomno [19] pointed out that the first part of the waveform could be described in terms essentially of a flat space “quadrupole formula” for a test particle following a Schwarzschild dynamics (Ruffini-Wheeler approximation [20]), while the last part of the waveform was dominated by exponentially damped harmonic oscillations. These damped oscillations were interpreted by Press [21] (see also Vishveshwara [22]) as vibrational modes (now called quasi-normal modes) of a Schwarzschild black hole. The perturbative formalism employed in these works has been later shown to be expressible in a gauge invariant manner [23, 24, 25, 26]. The case of a particle plunging from infinity with *nonzero angular momentum* has been discussed by Detweiler and Szedenits [27] and Oohara and Nakamura [28] by means of the curvature perturbation formalism of Teukolsky [29]. The radial plunge problem has been recently extended to a plunge from a finite distance [30, 31], with particular emphasis on the effect of the choice of initial data.

However, none of the above works has studied the *transition* from the quasi-circular adiabatic inspiral phase to the plunge phase in extreme-mass-ratio binary black hole systems. The reason is that the original Regge-Wheeler-Zerilli test-particle approach seems to require the test particle to follow an exact *geodesic* of the Schwarzschild background. Here we shall bypass this stumbling block by appealing to some results of PN theory. In particular, the Effective One Body (EOB) approach to the general relativistic two body dynamics, which has been recently proposed to study the transition from inspiral to plunge in the comparable-mass case [11, 12, 34, 35, 36, 37], describes the dynamics of a binary system in terms of two separate ingredients: (i) a Hamiltonian $H_{\text{EOB}}(M, \mu)$ describing the *conservative* part of the relative dynamics, and (ii) a non-Hamiltonian supplementary force $\mathcal{F}_{\text{EOB}}(M, \mu)$ approximately describing the reaction to the loss of energy and angular momentum along quasi-circular orbits. Following a prescription suggested in [10] the badly convergent [38] PN-Taylor series giving the angular momentum flux is *resummed* by means of Padé approximants.

Our general motivation for studying this problem is: (i) to gain information on black hole plunges in a regime ($\mu \ll M$) that is not yet accessible to full numerical simulations, and (ii) to learn how to match analytical results to numerical ones in a situation where it is relatively easy to perform many, controllable high-accuracy numerical simulations. This paper will be mainly devoted to the discussion of our numerical framework; see [40] for a thorough comparison between analytical and numerical results.

2. Relative dynamics of extreme-mass-ratio binary black holes

In the EOB approach the relative dynamics of a binary system of masses m_1 and m_2 is described by a Hamiltonian $H_{\text{EOB}}(M, \mu)$ and a radiation reaction force $\mathcal{F}_{\text{EOB}}(M, \mu)$, where $M \equiv m_1 + m_2$ and $\mu \equiv m_1 m_2 / M$. In the general comparable-mass case H_{EOB} has the structure $H_{\text{EOB}}(M, \mu) = M \sqrt{1 + 2\nu(\hat{H}_\nu - 1)}$ where $\nu \equiv \mu/M \equiv m_1 m_2 / (m_1 + m_2)^2$ is the symmetric mass ratio. In the test mass limit that we are considering, $\nu \ll 1$, we can expand H_{EOB} in powers of ν . After subtracting inessential constants we get a Hamiltonian per unit (μ) mass $\hat{H} = \lim_{\nu \rightarrow 0} (H - \text{const.}) / \mu = \lim_{\nu \rightarrow 0} \hat{H}_\nu$ of the form

$$\hat{H} = \sqrt{A(\hat{r}) \left(1 + \frac{p_r^2}{B(\hat{r})} + \frac{p_\varphi^2}{\hat{r}^2} \right)}. \quad (1)$$

Here we have introduced the dimensionless variables $\hat{r} \equiv r/M$, $p_r \equiv \hat{P}_r \equiv P_r/\mu$ and $p_\varphi \equiv \hat{P}_\varphi/M \equiv P_\varphi/(\mu M)$. The functions $A(\hat{r}, \nu)$ and $B(\hat{r}, \nu)$ entering the Hamiltonian \hat{H}_ν are metric coefficients entering the effective one body metric

$$ds^2 = g_{\mu\nu} dx^\mu dx^\nu = -A(\hat{r}, \nu) dt^2 + B(\hat{r}, \nu) dr^2 + r^2 (d\theta^2 + \sin^2 \theta d\varphi^2) . \quad (2)$$

In the limit $\nu \rightarrow 0$ in which we shall use (1) the effective metric functions $A(\hat{r}, \nu)$ and $B(\hat{r}, \nu)$ reduce to the well-known Schwarzschild expressions $A(\hat{r}, 0) = (B(\hat{r}, 0))^{-1} = 1 - 2/\hat{r}$. Since the radiation generation process will be studied in terms of the Regge-Wheeler tortoise coordinate $r_* = r + 2M \log(r/(2M) - 1)$, it is useful to have the Hamiltonian explicitly written in terms of r_* and its conjugate momentum p_{r_*} . This amounts to performing a canonical transformation $(\hat{r}, p_r) \rightarrow (\hat{r}_*, p_{r_*})$. The invariance of the action, $p_{r_*} d\hat{r}_* = p_r d\hat{r}$ yields $p_r = (d\hat{r}_*/d\hat{r}) p_{r_*} = A^{-1} p_{r_*}$, so that the new Hamiltonian function becomes

$$\hat{H}(\hat{r}_*, p_{r_*}) = \sqrt{A \left(1 + \frac{p_\varphi^2}{\hat{r}^2} \right) + p_{r_*}^2} . \quad (3)$$

Hamilton's canonical equations in the equatorial plane ($\theta = \pi/2$) yield

$$\dot{\hat{r}}_* = \frac{p_{r_*}}{\hat{H}} , \quad (4)$$

$$\dot{\hat{r}} = \frac{A}{\hat{H}} p_{r_*} \equiv v_r , \quad (5)$$

$$\dot{\varphi} = \frac{A}{\hat{H}} \frac{p_\varphi}{\hat{r}^2} \equiv \omega , \quad (6)$$

$$\dot{p}_{r_*} = - \frac{\hat{r} - 2}{\hat{r}^3 \hat{H}} \left[p_\varphi^2 \left(\frac{3}{\hat{r}^2} - \frac{1}{\hat{r}} \right) + 1 \right] , \quad (7)$$

$$\dot{p}_\varphi = \hat{\mathcal{F}}_\varphi \equiv - \frac{32}{5} \nu \omega^5 \hat{r}^4 \frac{\hat{f}_{\text{DIS}}(\omega \hat{r})}{1 - \sqrt{3} \omega \hat{r}} . \quad (8)$$

On the r.h.s. of the last equation we have introduced the second ingredient of the EOB approach: the radiation reaction force $\hat{\mathcal{F}}_\varphi$. The function $\hat{f}_{\text{DIS}}(\omega \hat{r})$ is the “factored flux function” of [10] scaled to the Newtonian (quadrupole) flux. Reference [10] has shown that the sequence of near-diagonal Padé approximants of $\hat{f}_{\text{DIS}}(\omega \hat{r})$ exhibits, during the quasi-circular inspiral phase ($\hat{r} > 6$), a good convergence toward the exact result known numerically [38] in the $\nu \rightarrow 0$ limit. Here we shall use the $\nu \rightarrow 0$ limit of the 2.5 PN accurate $\hat{f}_{\text{DIS}}(\omega \hat{r})$ (i.e., equations (3.28)-(3.36) of [12] in the $\nu = 0$ limit). Following the suggestion of [37], we expressed, in (8), $\hat{\mathcal{F}}_\varphi$ as a function of the two variables ω and \hat{r} with the hope that this expression remains approximately valid during the plunge ($\hat{r} < 6$). We shall give evidence below that this hope is fulfilled. Note also that the flux used in constructing $\hat{\mathcal{F}}_\varphi$, in (8), refers to the momentum flux *at infinity*. Reference [39] has shown that the flux down the event horizon (of the background Schwarzschild black hole of mass M) would correspond to a (here negligible) 4 PN effect.

2.1. Quasi-circular orbits and transition from inspiral to plunge

Following Section IV(A) of [12] and taking the $\nu \rightarrow 0$ limit in all terms except the crucial $\hat{\mathcal{F}}_\varphi = \mathcal{O}(\nu)$, we start the orbit at some given initial radius \hat{r} and initial phase φ with corresponding momenta:

$$p_\varphi \equiv \dot{J}_{\text{adiab}} = \frac{\hat{r}}{\sqrt{\hat{r} - 3}} , \quad (9)$$

$$p_r = - \frac{1}{C_r} \frac{B_r}{\omega_r^2} , \quad (10)$$

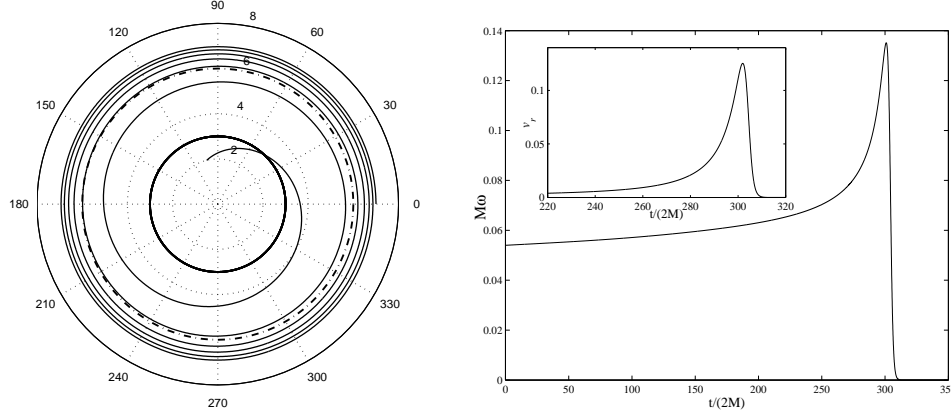


Figure 1. *Left panel:* Plunge relative orbit from $r = 7M$. The circle represented with a thick dashed line is the LSO at $r = 6M$. The thick solid line circle represents the light ring at $r = 3M$. *Right panel:* Radial velocity $v_r = \dot{r}$ and orbital angular frequency $\omega = \dot{\varphi}$ versus coordinate time.

where we explicitly have (with $\hat{H}_0 \equiv \hat{H}(p_r = 0)$)

$$C_r = \frac{A^2(\hat{r})}{\hat{H}_0}, \quad (11)$$

$$\omega_r^2 = \frac{1}{(\hat{H}_0)^2} A^2(\hat{r}) \frac{\hat{r} - 6}{\hat{r}^3(\hat{r} - 3)}, \quad (12)$$

$$B_r = -\frac{2j_{\text{adiab}}}{(\hat{H}_0)^2} A^2(\hat{r}) \frac{\hat{r} - 3}{\hat{r}^4} \hat{\mathcal{F}}_\varphi, \quad (13)$$

Figure 1 shows the trajectory determined by this kind of initial $\hat{r} = 7$, $\varphi = 0$ and $\nu = 0.01$ (for the sake of convenience we fix $M = 1$ in the numerical calculations); after ~ 5 orbits the trajectory crosses the Last Stable Orbit (LSO) at $\hat{r} = 6$ and then “plunges” (in a quasi-circular way $v_r \ll 1$, see inset in the right panel) into the black hole. It has to be noted that the orbital angular frequency $M\omega$ reaches a sharp maximum nearly at the light ring crossing ($\hat{r} = 3$).

3. Gravitational wave generation in the extreme mass ratio limit

We now complete the description of an extreme-mass-ratio binary system by computing the gravitational wave emission driven by the system during the inspiral and the plunge.

Let us recall that non-spherical linear metric perturbations around a Schwarzschild black hole can be expanded in scalar, vector and tensor spherical harmonics that are called even-parity [or odd-parity] if they transform under parity as $(-1)^\ell$ [or $(-1)^{\ell+1}$] and are decoupled because the black hole is non rotating. The seven even-parity metric multipoles [or the three odd-parity multipoles] can be combined together so that Einstein equations yield a wave-like equation for the even-parity [or odd-parity] gauge-invariant master variable $\Psi_{\ell m}^{(e)}$ [or $\Psi_{\ell m}^{(o)}$] with corresponding (Zerilli-Moncrief/Regge-Wheeler) potential $V_\ell^{(e/o)}$. In Schwarzschild coordinates and in the presence of a general matter source driving the perturbation of the spacetime, they read

$$\partial_t^2 \Psi_{\ell m}^{(e/o)} - \partial_{r_*}^2 \Psi_{\ell m}^{(e/o)} + V_\ell^{(e/o)} \Psi_{\ell m}^{(e/o)} = S_{\ell m}^{(e/o)}. \quad (14)$$

The well-known expressions of the potentials and the less well-known expressions of the sources for a general stress-energy tensor can be found in [25, 26]. We recall that from $\Psi_{\ell m}^{(e)}$ and $\Psi_{\ell m}^{(o)}$ one can easily obtain, when considering the limit $r \rightarrow \infty$, the h_+ and h_\times gravitational-wave polarization amplitude, and the emitted power and angular momentum flux according to

$$h_+ - ih_\times = \frac{1}{r} \sum_{\ell \geq 2, m} \sqrt{\frac{(\ell+2)!}{(\ell-2)!}} \left(\Psi_{\ell m}^{(e)} + i\Psi_{\ell m}^{(o)} \right) {}_{-2}Y^{\ell m}, \quad (15)$$

$$\dot{E} = \frac{1}{16\pi} \sum_{\ell \geq 2, m} \frac{(\ell+2)!}{(\ell-2)!} \left(\left| \dot{\Psi}_{\ell m}^{(o)} \right|^2 + \left| \dot{\Psi}_{\ell m}^{(e)} \right|^2 \right), \quad (16)$$

$$\dot{J} = \frac{1}{32\pi} \sum_{\ell \geq 2, m} \left\{ im \frac{(\ell+2)!}{(\ell-2)!} \left[\dot{\Psi}_{\ell m}^{(e)} \Psi_{\ell m}^{(e)*} + \dot{\Psi}_{\ell m}^{(o)} \Psi_{\ell m}^{(o)*} \right] + c.c. \right\}. \quad (17)$$

where the overdot stands for time-derivative and ${}_{-2}Y^{\ell m} \equiv {}_{-2}Y^{\ell m}(\theta, \varphi)$ are the $s = 2$ spin-weighted spherical harmonics [41]. In our physical setting ($\nu \rightarrow 0$) the sourcing stress-energy tensor is, to leading order, that of a test particle following the (relative) dynamics described above. We can then use the gauge-invariant multipoles of the stress-energy tensor of a point particle as explicitly given in Appendix A of [26]. Since the Zerilli-Moncrief and Regge-Wheeler equations are solved on a r_* grid, it is natural to express the source in terms of $\delta(r_* - R_*(t))$ where $R_*(t)$ denotes the “particle tortoise coordinate”, by contrast to a general “field coordinate” r_* . In addition, since the particle dynamics is written using canonical variables, it is also natural to express the source in terms of the particle coordinates R_* and Φ and their (rescaled) conjugate momenta \hat{P}_{R_*} and \hat{P}_φ . This has the advantage [over the use of the r coordinate and $\delta(r - R(t))$] of allowing one to push the evolution in time as much as one as one wants when $r \rightarrow 2M$, without introducing spurious boundary effects that may spoil the waveforms (and in particular the late-time tail). The coordinate transformation $r \rightarrow r_*$ (with $dr/dr_* = 1 - 2M/r = A(r)$) implies the relations

$$\delta(r - R(t)) = A(r)^{-1} \delta(r_* - R_*(t)), \quad (18)$$

$$\partial_r \delta(r - R(t)) = -\frac{2M}{A(r)^2 r^2} \delta(r_* - R_*(t)) + \frac{1}{A(r)^2} \partial_{r_*} \delta(r_* - R_*(t)). \quad (19)$$

Straightforward algebra permits then to derive from the results of [26] the following explicit expressions for the source terms in (14)

$$\begin{aligned} S_{\ell m}^{(e)} = & -\frac{16\pi\mu Y_{\ell m}^*}{r\hat{H}\lambda[(\lambda-2)r+6M]} \left\{ \left(1 - \frac{2M}{r}\right) (\hat{P}_\varphi^2 + r^2) \partial_{r_*} \delta(r_* - R_*(t)) \right. \\ & + \left\{ -2im \left(1 - \frac{2M}{r}\right) \hat{P}_{R_*} \hat{P}_\varphi + \left(1 - \frac{2M}{r}\right) \left[3M \left(1 + \frac{4\hat{H}^2 r}{(\lambda-2)r+6M}\right) \right. \right. \\ & - \frac{r\lambda}{2} + \frac{\hat{P}_\varphi^2}{r^2(\lambda-2)} [r(\lambda-2)(m^2 - \lambda - 1) + 2M(3m^2 - \lambda - 5)] \\ & \left. \left. + (\hat{P}_\varphi^2 + r^2) \frac{2M}{r^2} \right] \right\} \delta(r_* - R_*(t)) \Big\}, \quad (20) \end{aligned}$$

$$S_{\ell m}^{(o)} = \frac{16\pi\mu\partial_\theta Y_{\ell m}^*}{r\lambda(\lambda-2)} \left\{ \left[\left(\frac{\hat{P}_{R_*} \hat{P}_\varphi}{\hat{H}} \right)_{,t} - 2\hat{P}_\varphi \frac{r-2M}{r^2} - im \frac{r-2M}{r^3} \frac{\hat{P}_{R_*} \hat{P}_\varphi^2}{\hat{H}^2} \right] \delta(r_* - R_*(t)) \right\}$$

$$+ \left(1 - \frac{P_{R_*}^2}{\hat{H}} \right) \hat{P}_\varphi \partial_{r_*} \delta(r_* - R_*(t)) \Big\} , \quad (21)$$

where $\lambda \equiv \ell(\ell + 1)$. In the above equations we have chosen to write the sources in the functional form

$$S_{\ell m}^{(e/o)} = G_{\ell m}^{(e/o)}(r, t) \delta(r_* - R_*(t)) + F_{\ell m}^{(e/o)}(r, t) \partial_{r_*} \delta(r_* - R_*(t)) , \quad (22)$$

with r -dependent (rather than $R(t)$ -dependent) coefficients $G(r)$, $F(r)$. Note that the time dependence of $F(r, t)$ and $G(r, t)$ comes from the dependence on \hat{H} , \hat{P}_{R_*} and \hat{P}_φ . By exploiting the properties of the δ -function, we can also rewrite the sources in the functional form

$$S_{\ell m}^{(e/o)} = \tilde{G}_{\ell m}^{(e/o)}(R_*(t)) \delta(r_* - R_*(t)) + F_{\ell m}^{(e/o)}(R_*(t)) \partial_{r_*} \delta(r_* - R_*(t)) , \quad (23)$$

where

$$\tilde{G}_{\ell m}^{(e/o)}(R_*) = G_{\ell m}^{(e/o)}(R_*) - \left. \frac{dF_{\ell m}^{(e/o)}}{dr_*} \right|_{r_*=R_*} . \quad (24)$$

Expressions (22) and (23) are mathematically equivalent, for a distributional source, but become numerically (slightly) different when the δ -function is approximated on the r_* numerical domain by means of a narrow Gaussian.

4. Numerical framework, tests and comparison with the literature

4.1. Numerical procedure

We solve the equations given in section 2 for the particle dynamics using a standard fourth-order Runge-Kutta algorithm with adaptive stepsize [42]. Then we insert the resulting position and momenta in the source terms $S_{\ell m}^{(e/o)}$ using a Gaussian-function representation of $\delta(r_* - R_*(t))$ (see below). The corresponding Zerilli-Moncrief and Regge-Wheeler equations are then numerically solved, using standard techniques [42, 43], in the time domain (for each multipole (ℓ, m)) by discretizing the r_* axis ($r_* \in [r_*^{\min}, r_*^{\max}]$) with a uniform grid spacing Δr_* . In particular, the solution can be computed either by means of a centred second-order finite differencing algorithm, or by the following implementation of the Lax-Wendroff method (that is the one usually preferred). In this second case, it is convenient to rewrite the wave-equations as a first-order flux conservative system (with sources) in the form $\partial_t \mathbf{U} + \partial_{r_*} \mathbf{F} = \mathbf{S}$, where we have defined the vector of “conserved quantities” \mathbf{U} and the “fluxes” \mathbf{F} as

$$\mathbf{U} \equiv \begin{pmatrix} \Psi_{\ell m}^{(e/o)} \\ w \end{pmatrix} \quad \mathbf{F} \equiv \begin{pmatrix} \Psi_{\ell m}^{(e/o)} \\ -w \end{pmatrix} \quad (25)$$

where $w = \partial_t \Psi_{\ell m}^{(e/o)} + \partial_{r_*} \Psi_{\ell m}^{(e/o)}$ and the vector \mathbf{S} is

$$\mathbf{S} = \begin{pmatrix} w \\ V_\ell^{(e/o)} \Psi_{\ell m}^{(e/o)} + S_{\ell m}^{(e/o)} \end{pmatrix} , \quad (26)$$

Denoting by j the spatial grid-point index, n the time level and Δt the time step, the explicit time-advancing algorithm reads

$$\mathbf{U}_j^{n+1} = \mathbf{U}_j^n - \frac{\Delta t}{2\Delta r_*} [\mathbf{F}_{j+1}^n - \mathbf{F}_{j-1}^n] + \frac{\Delta t^2}{2\Delta r_*^2} [\mathbf{F}_{j+1}^n - 2\mathbf{F}_j^n + \mathbf{F}_{j-1}^n] \mathbb{A} + \Delta t \mathbf{S}_j^n , \quad (27)$$

where we introduced the matrix $\mathbb{A} \equiv \text{diag}(1, -1)$. This algorithm is stable under the standard Courant-Friedrichs-Levy [43] condition $\Delta t / \Delta r_* < 1$. We typically use $\Delta t / \Delta r_* = 0.9$.

On the boundaries we impose ingoing (at r_*^{\min}) and outgoing (at r_*^{\max}) standard Sommerfeld conditions. This efficiently suppress reflections from the boundaries apart from tiny effects that can modify (if we do not use sufficiently large grids) the power-law tail at the end of the black hole ringdown phase. [Improved non-reflecting boundary conditions for Zerilli-Moncrief and Regge-Wheeler equations have been recently discussed [44]].

4.2. Approximating the δ -function

We approximate the δ -function that appear in the source terms by a smooth function $\delta_\sigma(r_*)$ (and $\partial_{r_*}\delta(r_*)$ by $\partial_{r_*}\delta_\sigma(r_*)$). We use[‡]

$$\delta(r_* - R_*(t)) \rightarrow \frac{1}{\sigma\sqrt{2\pi}} \exp\left[-\frac{(r_* - R_*(t))^2}{2\sigma^2}\right], \quad (28)$$

with $\sigma \geq \Delta r_*$. In practice $\sigma \simeq \Delta r_*$ works well thanks to the effective averaging entailed by the fact that $R_*(t)$ is not restricted to the r_* grid, but varies nearly continuously on the r_* axis. In the continuum limit ($\sigma \simeq \Delta r_* \rightarrow 0$) the derivatives of both $\Psi_{\ell m}^{(e)}$ and $\Psi_{\ell m}^{(o)}$ would be discontinuous at the location of the particle $r_* = R_*$, generating numerical noise (Gibbs phenomenon) if standard numerical methods are used. However, the smoothing of $\delta(r_* - R_*(t))$, together with the use of a numerical method like Lax-Wendroff (that has a bit of numerical dissipation built in) avoids any problems related to high frequency oscillations and provides us with a clean and stable evolution §. The important scale in our problem is M which determines the “width” of the Zerilli potential. We found that a resolution of $\sigma \simeq \Delta r_* = 0.01M$ is small enough to ensure numerical convergence to the continuum solution.

4.3. Numerical tests: circular orbits and radial plunge

We have tested the reliability of our code by recomputing results for simple geodesic trajectories ($\dot{\mathcal{F}}_\varphi = 0$) that have been already obtained in the literature using both time-domain and frequency domain approaches, as well as different treatments for the particle and different expressions for the sources.

First of all we discuss the case of circular orbits. Table 1 lists the energy and angular momentum fluxes (at $r_{\text{obs}} = 1000M$) up to the $\ell = 4$ multipole for an orbit of radius $r = 7.9456$. This permits a direct comparison with the results of Martel [32] (see also [33]), that we include in the table as well for the sake of completeness. For this test run we consider a (relatively) coarse resolution of $\Delta r_* = 0.02M$; this is enough to have a very small difference with Martel results for the $\ell = 2$ multipoles, but the agreement obviously worsens for higher multipoles, for which it is necessary to increase the resolution. That is the reason why, when discussing the real plunge phenomenon driven by radiation reaction we shall use resolutions up to $\Delta r_* = 5 \times 10^{-3}$ to properly capture the behaviour of the highest multipoles.

Our second test concerns the waveform of a particle plunging radially into the black hole from a finite distance (where it starts at rest). This problem has received some attention in the recent literature [30, 31], thereby extending (by means of both frequency-domain and time domain approaches) the pioneering analysis of Davis *et al.* [18, 19] of the early 70s for a particle plunging from an infinite distance.

[‡] Note that this smoothing of the distributional stress-energy tensor into a formally extended one only concerns the calculation of the waveform. The dynamics, equations (4)-(8), is that of a δ -function stress-energy tensor. We use this smoothing only as a numerical technique, and we have checked that we were in the convergent regime.

§ Note that the use of a method without dissipation, like a standard leapfrog, introduces high frequency noise if σ is too small. For this reason we prefer to use the Lax-Wendroff technique for most of the simulations.

Table 1. Energy and angular momentum fluxes extracted at $r_{\text{obs}} = 1000M$ for a particle orbiting the black hole on a circular orbit of radius $r = 7.9456$. Comparison with the results of Martel [32].

ℓ	m	$(\dot{E}/\mu^2)_{\text{here}}$	$(\dot{E}/\mu^2)_{\text{Martel}}$	rel. diff.	$(\dot{J}/\mu^2)_{\text{here}}$	$(\dot{J}/\mu^2)_{\text{Martel}}$	rel. diff.
2	1	8.1998×10^{-7}	8.1623×10^{-7}	0.4%	1.8365×10^{-5}	1.8270×10^{-5}	0.5%
	2	1.7177×10^{-4}	1.7051×10^{-4}	0.7%	3.8471×10^{-3}	3.8164×10^{-3}	0.5%
3	1	2.1880×10^{-9}	2.1741×10^{-9}	0.6%	4.9022×10^{-4}	4.8684×10^{-8}	0.7%
	2	2.5439×10^{-7}	2.5164×10^{-7}	1.1%	5.6977×10^{-6}	5.6262×10^{-6}	1.2%
4	3	2.5827×10^{-5}	2.5432×10^{-5}	1.5%	5.7846×10^{-4}	5.6878×10^{-4}	1.7%
	1	8.4830×10^{-13}	8.3507×10^{-13}	1.6%	1.8999×10^{-11}	1.8692×10^{-11}	1.6%
4	2	2.5405×10^{-9}	2.4986×10^{-9}	1.7%	5.6901×10^{-8}	5.5926×10^{-8}	1.7%
	3	5.8786×10^{-8}	5.7464×10^{-8}	2.3%	1.3166×10^{-6}	1.2933×10^{-6}	1.8%
4	4	4.8394×10^{-6}	4.7080×10^{-6}	2.7%	1.0838×10^{-4}	1.0518×10^{-4}	3.0%

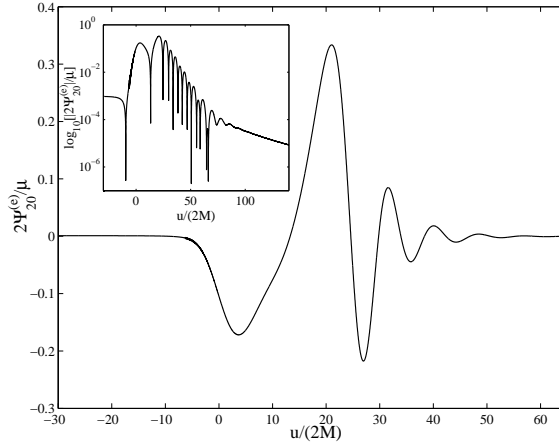


Figure 2. Test of the code: waveform (on a logarithmic scale in the inset) for a particle plunging radially on the black hole along the z -axis from $r = 10M$

We selected the same kind of initial data as described in references [30, 31], so as to have an initial profile of $\Psi_{\ell 0}^{(e)}$ that is conformally flat. However, since we have slightly “smeared” the δ -function, we cannot use the “discontinuous” analytical initial data of references [30, 31]. We numerically solve the Hamiltonian constraint by writing it as a tridiagonal system that is then solved using a standard LU decomposition. Figure 2 displays (for the case $\ell = 2$) the waveform generated by a particle plunging into the black hole along the z -axis, starting from rest at $r = 10M$. It has been extracted at $r_{\text{obs}} = 500M$ and is shown versus the retarded time $u = t - r_{\text{obs}}$. The master function $\Psi_{20}^{(e)}$ has been multiplied by a factor two (linked to a different choice of normalization in [30, 31]) to facilitate the (very satisfactory) comparison with the top-right panel of figure 4 in [31] or the top-left panel of figure 6 in [30]. We used a resolution of $\Delta r_* = 0.01M$ with $r_* \in [-800M, 1800M]$. This avoids the influence of the boundaries and allows one to capture the late-time non-oscillatory decay after the QNM ringdown phase (see the inset in figure 2).

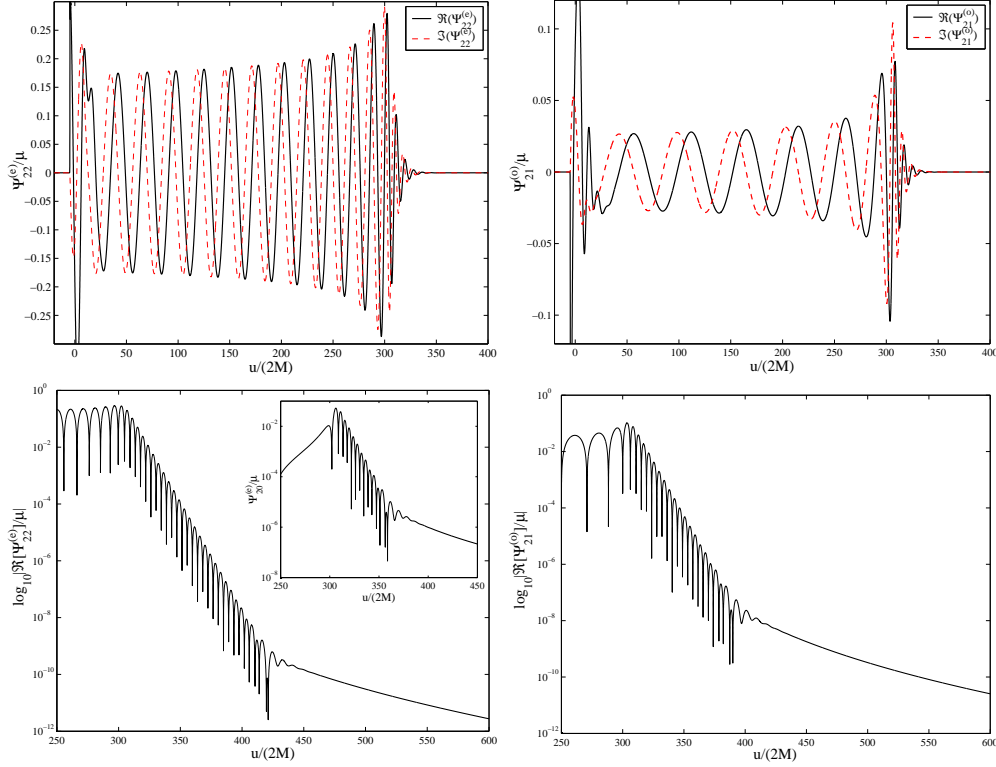


Figure 3. Dominant $\ell = m = 2$ even-parity *Left panel* and $\ell = 2, m = 1$ odd-parity *Right panel* gravitational wave multipoles generated by the quasi-circular plunge of a particle with $\nu = 0.01$ initially at $r = 7M$.

5. Transition from inspiral to plunge: waveforms

Now that we have shown that our code can reproduce with good accuracy known results for geodesic orbits, let us break new ground by considering the waveform emitted during the transition from inspiral to plunge. We refer here to the dynamics described in section 2.1; *i.e.*, the particle with $\nu = 0.01$ is initially at $r = 7M$ with dynamical initial data defined by the quasi-circular (adiabatic) approximation described there. We also need initial data for the field perturbations: $\Psi_{\ell m}^{(e/o)}$, $\partial_t \Psi_{\ell m}^{(e/o)}$. To do so, one should in principle select the solution of the perturbed Hamiltonian and momentum constraints which corresponds to the physically desired “no-incoming radiation condition”. However, we took a more pragmatic approach. As it is often done in the literature, we impose $\Psi_{\ell m}^{(e/o)} = \partial_t \Psi_{\ell m}^{(e/o)} = 0$ at $t = 0$. This “bad” choice of initial data produces an initial burst of unphysical radiation, but after a while the gravitational waveform is driven by the motion of the source so that it is sufficient not to include the early part of the waveform in the final analysis. Figure 3 depicts the dominant $\ell = 2$ waveforms ($m = 2$ and $m = 1$ multipoles) extracted at $r_{\text{obs}} = 250M$. For the sake of comparison we normalize the waveforms to the mass μ (see below a discussion of the approximate universality of this scaled waveform). The numerical grid we adopted for this simulation was $r_* \in [-1200M, 1200M]$ with resolution $\Delta r_* = 0.01M$. As we were

Table 2. Total energy and angular momentum extracted at $r_{\text{obs}} = 250M$ for the “plunge phase” ($r < 5.9865M$) of a dynamics with $\nu = 0.01$.

ℓ	m	$M\Delta E/\mu^2$	$\Delta J/\mu^2$
2	0	9.8×10^{-4}	0
	1	2.06×10^{-2}	0.084
	2	3.31×10^{-1}	2.994
3	0	3.4×10^{-5}	0
	1	5.6×10^{-4}	1.2×10^{-3}
	2	8.1×10^{-3}	3.9×10^{-2}
	3	1.05×10^{-1}	8.5×10^{-1}
4	0	1.7×10^{-6}	0
	1	2.4×10^{-5}	3.6×10^{-5}
	2	3.3×10^{-4}	1.1×10^{-3}
	3	3.5×10^{-3}	1.8×10^{-2}
	4	4.2×10^{-2}	3.2×10^{-1}

mentioning above, after an initial unphysical burst of radiation the gravitational waveforms are driven by the motion of the particle during the quasi-circular inspiral and plunge. From the inspection of the particle dynamics we described above, we know it crosses the LSO at $u/(2M) \simeq 240$ and passes through the light ring (where the gravitational perturbation driven by the source is filtered by the peak of the potential) at $u/(2M) \simeq 300$ (where both the orbital frequency ω and the radial velocity v_r have a maximum). Both $\Psi_{22}^{(e)}$ and $\Psi_{21}^{(o)}$ show a progressive increase in frequency and amplitude until $u/(2M) \simeq 300$, where a maximum of amplitude is reached. Then follows a QNM dominated ringdown phase.

To validate our results, we study the convergence of the waveforms by considering resolutions $\Delta r_* = (0.02, 0.01, 0.005)$. For the dominant $\ell = m = 2$ waveforms we found a convergence rate $\beta \simeq 1.6$, defined from $\Delta\Psi \propto \Delta r_*^\beta$. Here $\Delta\Psi$ is defined as the discretized root mean square between the waveform at the resolution Δr_* and the highest resolution one. Generally speaking, a resolution $\Delta r_* = 0.01$ is sufficient to determine the energy and angular momentum radiated with an accuracy that is of the order of 1% (or better) for the quadrupole modes. Having the same accuracy for higher modes needs to increase the resolution; however, we have verified that this is sufficient for having an accuracy (for the energy) that is not worse than 6% for the other multipoles up to $\ell = 4$ (the most sensitive one being $\ell = 4, m = 0$).

To give some numbers we computed the total energy and angular momentum loss during what might (approximately) be called the plunge phase (that is, after the crossing of the LSO at $6M$). More precisely, we selected the part of the waveform for $u/(2M) \geq 240$ which corresponds to radii $\hat{r} \leq 5.9865$. Table 2 lists the partial multipolar energy and angular momentum losses up to $\ell = 4$. These values were computed with resolution $\Delta r_* = 0.01$ so that the accuracies are of the order of 1% for $\ell = 2$, 2–4% for $\ell = 3$ and of 5–6% for $\ell = 4$. When one sums all the multipoles, the total energy emitted is found to be $M\Delta E/\mu^2 \simeq 0.51$ and $\Delta J/\mu^2 \simeq 4.3$. Only for the sake of comparison, let us mention that this “plunge” $M\Delta E/\mu^2$ is about 50 times larger than the “radial” (Davis *et al.* [18, 19]) one (summed up to $\ell = 4$) which amounts to $M\Delta E/\mu^2 = 0.0104$ (for a plunge from infinity).

An important consistency check of our approach (which assumes the specific PN-resummed radiation reaction force (8)) is to compare the angular momentum loss assumed in the dynamics, *i.e.* $-(dP_\varphi/dt)/(\mu M) = -\hat{\mathcal{F}}_\varphi$, to the angular momentum flux radiated by the multipolar gravitational waves $\Psi_{\ell m}^{(e/o)}$ at infinity (up to $\ell = 4$). The left panel of figure 4 displays $-(dP_\varphi/dt)/(\mu M)$ (dashed line) versus $(dJ/dt)_{\text{gw}}/(\mu M)$ (solid line) up to

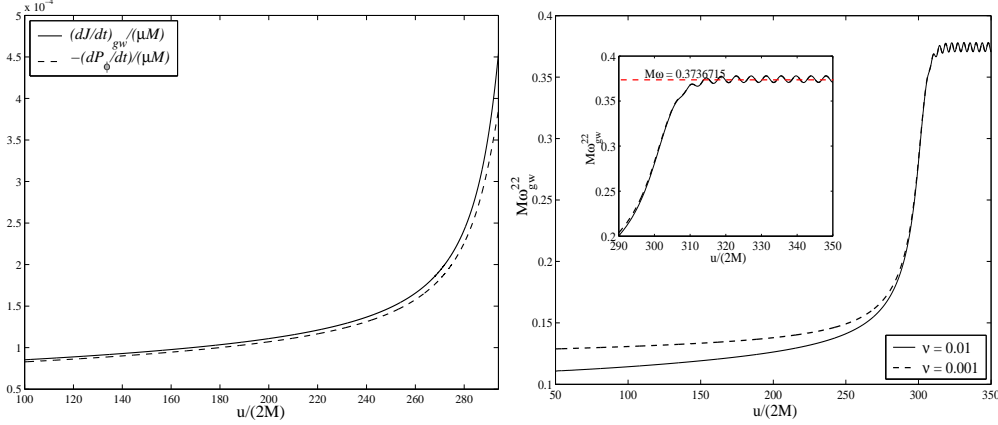


Figure 4. *Left panel:* angular momentum flux computed from the gravitational waveform compared to the angular momentum loss assumed in the dynamics with $\nu = 0.01$. *Right panel:* Instantaneous gravitational wave frequency for two values of ν . The signal is “approximately universal” after $u/(2M) \simeq 280$, which roughly corresponds to $r \lesssim 5.15$ (“quasi-geodesic plunge”). After $u/(2M) \simeq 300$ starts the QNM phase.

roughly the crossing of the light ring. The very good agreement between the two curves is a confirmation of the good convergence of the Padé-resummed radiation reaction force $\hat{\mathcal{F}}_{\varphi}$, equation (8), toward the exact result. This confirmation goes beyond the tests of [10] which were limited to the inspiral phase $\hat{r} > 6$. The retarded times $240 \lesssim u/(2M) \lesssim 290$ in figure 4 correspond to the plunge phase [the merger (matching) occurring at $u/(2M) \sim 300$].

The question that one can ask at this point is how much the numbers of table 2 are universal. Let us first recall that [12] has shown that the transition between inspiral and plunge was taking place in a radial domain around the LSO which scaled with ν as $r - 6M \sim \pm 1.89M\nu^{2/5}$, with radial velocity scaling as $v_r \sim -0.072\nu^{3/5}$. The specific power $2/5$ -th appearing in the radial scaling yields, in the numerical case $\nu = 0.01$ that we consider in most of this paper, $r - 6M \sim \pm 0.30M$. This means that, formally, when $\nu = 0.01$, it is only when $6M - r \gg 0.3M$ that we can expect the plunge dynamics to become universal, in the sense that it will approach the geodesic which started from the LSO in the infinite past with zero radial velocity. If we wanted to reach this universal behaviour just below the LSO (say, for $r \leq 5.98$) we would need to use much smaller values of ν (say $\nu \lesssim 10^{-5}$). For larger values of ν we can only hope to see an approximate convergence to universal behaviour near the end of the plunge. This is illustrated in the right panel of Figure 4. This figure plots, versus retarded time u , the instantaneous gravitational wave frequency $M\omega_{\text{gw}}^{22}$, where ($\Im \equiv$ imaginary part)

$$M\omega_{\text{gw}}^{\ell m} = -\Im \left(\frac{\dot{\Psi}_{\ell m}^{(e/o)}}{\Psi_{\ell m}^{(e/o)}} \right) \quad (29)$$

for $\nu = 0.01$ (solid line) and $\nu = 0.001$ (dashed line). At early times, that is when the particle moves along a quasi-circular orbit, one has $M\omega_{\text{gw}}^{\ell m} \simeq mM\omega = 2M\omega$; i.e., the double of the orbital frequency. Then one has the transition regime mentioned above around the crossing of the LSO, i.e., for $u/(2M) \simeq 240$. The quasi-universal, quasi-geodesic plunge mentioned above starts afterwards around $u/(2M) \simeq 280$, i.e., $r \simeq 5.15M$ (for $\nu = 0.01$)

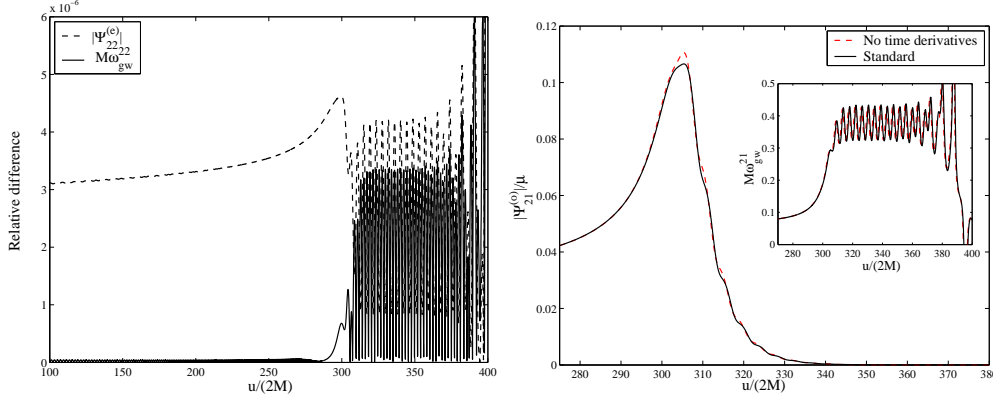


Figure 5. Consistency checks of the sources. *Left panel:* relative difference between waveforms obtained with different expressions for $S_{22}^{(e)}$. *Right panel:* check of the smallness of the effects linked to the terms $\propto \dot{P}_\varphi$ and $\propto \dot{H}$ in the odd-parity source $S_{21}^{(o)}$ from (21).

Then, after crossing the light ring, one enters another universal phase: the QNM one. In this QNM phase the gravitational wave angular frequency saturates and oscillates around the value $M\omega_{\text{gw}}^{22} = 0.3736715$ (highlighted in the inset). The fine structure of this gravitational wave frequency plot will be further discussed in [40].

We conclude this section by briefly quoting two consistency checks of the matter source that we have performed. The first check concerns the consistency between the two different functional forms (22) or (23) that the sources can take. As said above these two forms would be mathematically equivalent for a real δ -function, but will differ when using the Gaussian approximation (28). The left panel of figure 5 shows the relative difference between two gravitational wave moduli $|\Psi_{22}^{(e)}|$ (dotted line): one of them computed using (22) and the other using (23) with $\Delta r_* = 0.02$ and $\sigma = \Delta r_*$. This left panel also shows the difference between the gravitational wave frequencies $M\omega_{\text{gw}}^{22}$ (solid line) computed with the two different sources. The relative difference $\simeq 10^{-5}$ on both makes us confident that the “smeared” δ -function is a very good approximation to the actual δ -function. [Let us also comment, in passing, that we did a convergence check (for $\ell = m = 2$) by comparing waveforms obtained by means of Gaussians (with $\sigma = \Delta r_*$ and $\sigma = 2\Delta r_*$), finding a relative difference of the same order of magnitude $\simeq 10^{-5}$].

Finally, we performed a consistency check regarding the explicit time derivative appearing in the coefficient of $\delta(r_* - R_*(t))$ in the odd-parity source $S_{21}^{(o)}$ from (21). When expanded by Leibniz rule, this time derivative generates three terms. The term proportional to \dot{P}_{R_*} would be present along a geodesic motion. By contrast, the terms proportional to \dot{P}_φ and \dot{H} are proportional to ν and therefore vanish in the geodesic motion limit. These last two terms generate a correction of order $\mathcal{O}(\mu)\mathcal{O}(\nu) \propto \nu^2$ in the source. Such terms are *formally* negligible in the extreme mass ratio limit that we consider here. In the right panel of figure 5 we have checked to what extent these terms are *numerically* small.

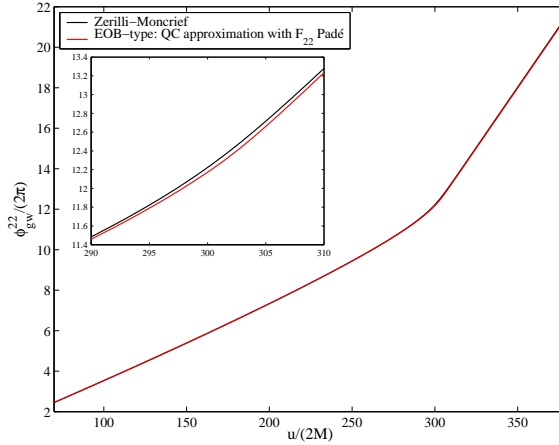


Figure 6. Comparison between the gravitational-wave phase for $\ell = m = 2$ obtained from the Zerilli-Moncrief equation or from analytically matching a 3PN improved quadrupole-type formula (factor F_{22} Padé) to a superposition of quasi-normal modes.

6. Conclusions

As we briefly mentioned in the Introduction, beyond solving for the first time, within a certain approximation, the problem of the plunge in the extreme mass ratio limit, the most important aim of this work was to build “actual” *numerical* waveforms to be then compared with *analytical* ones, within the EOB framework and philosophy.

We recall that the basic idea of the EOB framework is to produce quasi-analytical waveforms by patching together a quadrupole-type waveform during the inspiral and plunge to a QNM-type waveform after merger. In [40] we will use the numerical tools presented here to measure to what extent these EOB-type waveforms can approximate actual waveforms of binary black hole merger in the extreme mass ratio limit. We give an example of this numerical-analytical comparison in figure 6. This figure compares the phases of the gravitational waveforms obtained by two different methods, one numerical and the other semi-analytical. In the first method, the phase has been computed by integrating in time the instantaneous gravitational wave frequency given by (29), with $\Psi_{22}^{(e)}$ obtained by numerically solving the Zerilli-Moncrief equation. The second method computes an approximate waveform in the following way: Before crossing the light ring one uses a (Padé-resummed) 3PN-improved quadrupole-type formula to compute the waveform from the EOB dynamics. After crossing the light ring, the previous quadrupole-type signal, taken in the quasi-circular (QC) approximation, is *matched* to a superposition of the first five QNMs of the black hole. Then one computes the phase of this matched analytical waveform by integrating the corresponding instantaneous gravitational wave frequency. The agreement between the “actual” phase and the “effective one body” phase is impressively good: it turns out that the maximum difference between the two is less than 3% of a cycle.

Acknowledgments

We are grateful to E. Berti, A. Buonanno, R. De Pietri and L. Rezzolla for discussions. A.N. is supported by a post-doctoral fellowship of Politecnico di Torino. The computations were

performed on the INFN beowulf cluster for Numerical Relativity *Albert* at the University of Parma. A.N. gratefully acknowledges the support of ILIAS and IHES for hospitality during the completion of this work.

References

- [1] Pretorius F, 2005 *Phys. Rev. Lett.* **95**, 121101
- [2] Campanelli M, Lousto C O, Marronetti P, and Zlochower Y, 2006 *Phys. Rev. Lett.* **96** 111101
- [3] Baker J G, Centrella J, Choi D I, Koppitz M, and van Meter J, 2006 *Phys. Rev. Lett.* **96** 111102
- [4] Campanelli M, Lousto C O, and Zlochower Y, 2006 *Phys. Rev. D* **74**, 084023
- [5] Gonzalez J A, Sperhake U, Bruegmann B, Hannam M and Husa S, 2006, unpublished *arXiv:gr-qc/0610154*
- [6] Damour T, Jaranowski P and Schafer G, 2001 *Phys. Lett. B* **513**, 147
- [7] Blanchet L, Damour T, and Esposito-Farese G, 2004 *Phys. Rev. D* **69**, 124007
- [8] Blanchet L, Damour T, Esposito-Farese G and Iyer B R, 2005 *Phys. Rev. D* **71**, 124004
- [9] Blanchet L, 2006, *Living Rev. Relativity* **9**, 4. URL: <http://www.livingreviews.org/lrr-2006-4>
- [10] Damour T, Iyer B R and Sathyaprakash B S, 1998 *Phys. Rev. D*, **57**, 885
- [11] Buonanno A and Damour T, 1999 *Phys. Rev. D* **59**, 084006
- [12] Buonanno A and Damour T, 2000 *Phys. Rev. D* **62**, 064015
- [13] Buonanno A, Cook G B, and Pretorius F, 2006 unpublished *gr-qc/0610122*
- [14] Baker J G, van Meter J R, McWilliams S T, Centrella J and Kelly B J, 2006 unpublished, *arXiv:gr-qc/0612024*.
- [15] Baker J G, McWilliams S T, van Meter J R, Centrella J, Choi D I, Kelly B J and Koppitz M, 2006 unpublished, *arXiv:gr-qc/0612117*.
- [16] Regge T and Wheeler J A, 1957 *Phys. Rev.* **108**, 1063
- [17] Zerilli F J, 1970 *Phys. Rev. Lett.* **24**, 737
- [18] Davis M, Ruffini R, Press W H, and Price R H, 1971 *Phys. Rev. Lett.* **27**, 1466
- [19] Davis M, Ruffini R, and Tiomno J, 1972 *Phys. Rev. D* **5**, 2932
- [20] Ruffini R and Wheeler J A, in *Proceedings of the Cortona Symposium on weak interactions*, edited by L. Radicati, (Accademia Nazionale dei Lincei, Rome, 1971)
- [21] Press W H, 1971 *Astrophys. J. Letts.* **170**
- [22] Vishveshwara C V, 1970 *Nature*, **227**, 936
- [23] Moncrief V, 1974 *Ann. Phys. (N.Y.)* **88**, 323
- [24] Sarbach O and Tiglio M, 2001 *Phys. Rev. D*, **64**, 084016
- [25] Martel K and Poisson E, 2005 *Phys. Rev. D* **71**, 104003
- [26] Nagar A and Rezzolla L, 2005 *Class. Q. Grav.* **22**, R167; erratum, **23**, 4297
- [27] Detweiler S L and Szedenits E, 1979 *Astrophys. J.* **231**, 211
- [28] Oohara K I and Nakamura T, 1983 *Prog. Theor. Phys.* **70** 757; 1983 *Phys. Lett. A* **94** 349
- [29] Teukolsky S, 1973 *Astrophys. J.* **185**, 635
- [30] Lousto C O and Price R H, 1997 *Phys. Rev. D*, **55** 2124; 1997 *Phys. Rev. D*, **56**, 6439
- [31] Martel K and Poisson E, 2001 *Phys. Rev. D* **66**, 084001
- [32] Martel K, 2005 *Phys. Rev. D* **69**, 044025
- [33] Sopuerta C F and Laguna P, 2006 *Phys. Rev. D* **73** 044028
- [34] Damour T, Jaranowski P, and Schafer G, 2000 *Phys. Rev. D* **62**, 084011
- [35] Damour T, 2001 *Phys. Rev. D* **64**, 124013
- [36] Buonanno A, Chen Y and Damour T, 2006 *Phys. Rev. D* **74**, 104005
- [37] Damour T and Gopakumar A, 2006 *Phys. Rev. D* **73**, 124006
- [38] Poisson E, 1995 *Phys. Rev. D* **52**, 5719; **55**, 7980
- [39] Poisson E and Sasaki M, 1995 *Phys. Rev. D* **51** 5753
- [40] Damour T and Nagar A, *in preparation*
- [41] Goldberg J N, MacFarlane J, Newman E T, Rohrlich F and Sudarsahn E C G, 1967 *J. Math. Phys.* **8**, 2155
- [42] Press W H, Teukolsky S A, Vetterling W T, and Flannery B P, 1992 *Numerical Recipes in FORTRAN: The art of scientific computing 2nd ed.*, (Cambridge University Press, Cambridge, England)
- [43] Gustafsson B, Kreiss H O, and Olinger J, 1995 *Time Dependent Problems and Difference Methods* (John Wiley & Sons Inc.)
- [44] Lau S R, 2005 *J. Math. Phys.* **46**, 102503